Journal of Vacuum Science
and Technology A

RESEARCH ARTICLE | AUGUST 28 2023

Density functional theory study on reaction mechanisms of Co(^{tbu2}DAD)$_2$ for area selective-atomic layer deposition of Co films on metal surfaces

Nickolas Ashburn ; Xiuyao Lang ; Sumeet Pandey ; Steven Wolf; Steve Kramer ; John Smythe; Gurtej Sandhu ; Charles Winter ; Andrew C. Kummel ; Kyeongjae Cho

Check for updates

J. Vac. Sci. Technol. A 41, 052403 (2023)
https://doi.org/10.1116/6.0002840

View Online
Export Citation
CrossMark

Articles You May Be Interested In

Classification of processes for the atomic layer deposition of metals based on mechanistic information from density functional theory calculations

J. Chem. Phys. (February 2017)

Precision defect engineering of metal/insulator/metal diodes using atomic layer deposition to localize Ni impurities in Al_2O_3 tunnel barriers

J. Appl. Phys. (April 2021)

16 October 2023 16:07:51


HIDEN ANALYTICAL
Instruments for Advanced Science
- Knowledge
- Experience
- Expertise
Click to view our product catalogue
Contact Hiden Analytical for further details:
www.HidenAnalytical.com
info@hiden.co.uk

Gas Analysis
- dynamic measurement of reaction gas streams
- catalysis and thermal analysis
- molecular beam studies
- dissolved species probes
- fermentation, environmental and ecological studies

Surface Science
- UHV TPD
- SIMS
- end point detection in ion beam etch
- elemental imaging - surface mapping

Plasma Diagnostics
- plasma source characterization
- etch and deposition process reaction kinetic studies
- analysis of neutral and radical species

Vacuum Analysis
- partial pressure measurement and control of process gases
- reactive sputter process control
- vacuum diagnostics
- vacuum coating process monitoring

JVST A
Journal of Vacuum Science & Technology A

ARTICLE

pubs.aip.org/avs/jva

Density functional theory study on reaction mechanisms of Co(^{tbu2}DAD)$_2$ for area selective-atomic layer deposition of Co films on metal surfaces

Cite as: J. Vac. Sci. Technol. A **41**, 052403 (2023); doi: 10.1116/6.0002840
Submitted: 18 May 2023 · Accepted: 24 July 2023 ·
Published Online: 28 August 2023

View Online Export Citation CrossMark

Nickolas Ashburn,[1,2] Xiuyao Lang,[1] Sumeet Pandey,[2,a)] Steven Wolf,[3] Steve Kramer,[2] John Smythe,[2] Gurtej Sandhu,[2] Charles Winter,[4] Andrew C. Kummel,[3] and Kyeongjae Cho[1,a),b)]

AFFILIATIONS

[1] Department of Materials Science and Engineering, University of Texas at Dallas, Richardson, Texas 75080
[2] Micron Technology Inc., Boise, Idaho 83707
[3] Materials Science and Engineering Program and Department of Chemistry and Biochemistry, University of California, San Diego, La Jolla, California 92093
[4] Department of Chemistry, Wayne State University, 5101 Cass Avenue, Detroit, Michigan 48202

[a)] **Authors to whom correspondence should be addressed:** spandey@micron.com and kjcho@utdallas.edu
[b)] **Present address:** office # NSERL 3.412, 800 W Campbell Rd, Richardson, TX 75080.

ABSTRACT

As electronic devices scale in size approaching nm scales, the smaller feature sizes become more difficult and expensive to pattern. The most common patterning technique currently used in microelectronics industry, ArF laser immersion lithography, requires more and more steps to pattern one layer, the smaller the pitch becomes. Area selective-atomic layer deposition (AS-ALD) is one possible solution that allows for both fewer patterning steps and smaller feature sizes. However, the fundamental mechanisms of surface selectivity and the role of reducers in ALD growth are not fully understood. This modeling work focuses on the detailed atomic scale processes of AS-ALD deposition of Co metal on various substrate surfaces. Co is of particular interest for its capability in reducing resistance of metal interconnects in back end of lines when replacing Cu lines below 16 nm in critical dimension, and such a small linewidth can be achieved by the AS-ALD growth of Co films. This work shows the mechanisms and properties associated with the growth of Co on various surfaces (Cu, Pt, Co, and SiO$_2$) as well as the role of a reducing agent in facilitating surface reactions during ALD processes. Density functional theory was used to describe the reaction mechanisms and accurately describe the system's energetic and electronic characteristics during the deposition process. These findings provide insight into the fundamental mechanisms of selective ALD growth on metal surfaces against oxide surfaces and the catalytic role of reducers in facilitating the kinetics of ALD precursor reactions on metal surfaces.

I. INTRODUCTION

The area selective-atomic layer deposition (AS-ALD) and chemical vapor deposition (CVD) of many 3d transition metals and other materials are becoming increasingly more important as devices scale down in size.[1–3] ALD has grown in popularity for its capabilities in depositing films with atomic level control, high conformality on three-dimensional surfaces, and selectivity toward the chemical environments of certain surfaces.[4–6] In addition to the favorable growth properties, AS-ALD aids in overcoming multiple issues stemming from the use of etchants, lift-off chemicals, and resist films found in conventional lithographic patterning processes. In the sub-tens-of-nanometers regime, anisotropic reactions during dry etching make lateral material removal significantly more challenging than vertical etching.[7] Etching-free ALD addresses this issue by introducing selectivity in surface reactions. Moreover, it offers enhanced compatibility with sensitive materials anticipated for future nanoelectronic devices, including organic layers, graphene, carbon nanotubes, and nanowires.[8] Furthermore, to achieve the high selectivity required for patterning films using AS-ALD, the ALD precursors and reactants must exhibit characteristics including high inherent selectivity toward the target substrate (against surrounding substrates) and a higher thermal stability than the ALD deposition temperature. Additionally, the use of a thermally driven ALD process is important as plasma-enhanced ALD can damage the surface of the substrate and result in poor coverage uniformity of high aspect ratio features.[9]

The use of ALD for Co-based films has grown in popularity because of the high substrate selectivity for certain precursors as well as high conformality and thermal stability. Additionally, Co deposition is important in many applications in microelectronics including vias, interconnects, contact materials, liners, caps, and magnetic materials.[10–14] Co has extensively been considered as a replacement for copper interconnects, an aid in the nucleation and growth of Cu on SiO_2 substrates, and a barrier for interconnect lines.[1,14,15] These metal films have typically been grown by physical and chemical deposition methods.[16–18] Recently, 1,4-di-tertbutyl-1,3-diazadiene, $Co(^{tbu2}DAD)_2$ or $(N_2C_{10}H_{20})_2Co$, has been used as an ALD precursor for the low-temperature thermal AS-ALD deposition of seed layer Co to assist in Cu nucleation.[19–23] Although many Co precursors have been studied for the ALD growth of Co films, $Co(^{tbu2}DAD)_2$ has been shown to grow highly conformal, selective, and self-limiting films below 250 °C; with the precursor-reactant combination of $Co(^{tbu2}DAD)_2$+ HCOOH or TBA (tertbutyl amine), an ALD growth occurs readily on metals surface, but is inhibited on insulators such as SiO_2. DFT simulation can provide insight into the mechanisms of surface selective growth by calculating the thermodynamic reaction energies on metal and insulator surfaces.[24–27] While many experimental studies have been done showing the selectivity and growth characteristics of Co films on various substrates, there has been little work describing the fundamental driving forces that promote or inhibit $Co(^{tbu2}DAD)_2$ decomposition and Co deposition at ALD growth temperature on these substrate surfaces. This work investigates the underlying mechanisms of surface selective growth and describes the fundamental thermodynamic and electronic properties which affect this surface selectivity.

During the AS-ALD growth of $Co(^{tbu2}DAD)_2$, a coreactant is used to facilitate the reaction kinetics of $Co(^{tbu2}DAD)_2$ to Co metal without having to exceed the molecule's decomposition temperature. It has been shown that reducers play an important role in assisting in the growth of Co films.[19–23] This work, therefore, studied the growth of Co films on SiO_2 and metals, as well as the role of a model coreactant, NH_3, and its effect on the reaction mechanism between $Co(^{tbu2}DAD)_2$ and the substrate surface. The inherent selectivity of the precursor and the coreactant are examined along with the electronic properties of the precursor and its interaction with the surface during deposition. The utilization of reducing agents aids in ligand removal from precursors, thereby promoting the deposition of Co films. These reaction-limiting characteristics are shown to dictate the growth of Co on various substrates.

II. THEORETICAL METHODOLOGY

Computational studies were performed through density functional theory using the Hubbard-U-corrected spin-polarized generalized gradient approximation (GGA) for exchange–correlation interactions in the Vienna *ab initio* Simulation Package (VASP) with plane-wave basis with an energy cutoff of 500 eV and projector augmented-wave pseudopotentials.[28–30] Perdew–Burke–Ernzerhof functional[31] was used to represent the exchange–correlation interaction. The pseudopotential valence-electron configurations are $3d^74s^2$ for Co, $3d^94s^2$ for Cu, $5d^86s^2$ for Pt, $2s^22p^3$ for N, and $2p^22s^2$ and $1s^1$ for H. Accurate energy calculations for elements with strongly correlated orbitals were achieved through the application of the GGA + U method.[28,29] The GGA + U methodology is employed for the Co metal to address the substantial errors encountered when calculating redox reaction energies using the GGA functional. We utilize a U value of 3.32 eV from the materials project data set, which is determined by fitting experimental reaction enthalpies of the reaction $6CoO + O_2 \rightarrow 2Co_3O_4$.[32,33] The calculated lattice constants for Co, Pt, and Cu in the face-centered-cubic (FCC) Bravais lattice are 3.49, 3.83, and 3.57 Å, respectively. We utilized the cubic phase[34] of SiO_2 with a calculated lattice constant of 7.45 Å. Each supercell calculation was relaxed to a force convergence of 0.001 eV nm^{-1}. The k-space sampling of the Brillouin zone was done using a Monkhorst Pack grid with a mesh density of 0.003 nm^{-1}. For reaction energy calculations, the metal close-packed (111) surfaces consist of three layers, whereas the SiO_2(001) surface with O termination is constructed with seven Si layers and has a thickness of 13.56 Å. Each calculation was done on a supercell with surface dimensions ranging from 8 × 8 to 16 × 16 Å depending on the reaction process. All atoms were allowed to relax in surface reaction simulations. Additionally, the top and bottom surfaces in each periodic supercell were spaced to a 15 Å distance in vacuum to prevent any periodic image interaction. To achieve more accurate total energies, the magnetic state of each material was considered and relaxed in its most preferable configuration. The energies calculated were at 0 K, thus bringing the zero-point energies (ZPE) into consideration. For the decomposition of $Co(^{tbu2}DAD)_2$ precursor on surfaces, these ZPE values have been ignored without changing the overall analysis. This is due to the small frequency loss (<0.1 eV) for two Co–N bonds dissociation at each step with respect to the large reaction energy (>1 eV).[35–38]

The formation energy of each reaction step was calculated by subtracting the substrate and gas phase reactants from the reacted supercell. Note that the formation energy is negative when the reaction is favorable. This definition can best be described by Eq. (1), where ΔE^f is the formation energy of a reaction step that is equal to the total energy of the reacted supercell, E^r, minus the substrate total energy, E^s, and the sum of the individual reactant energies, E_i, for each species i,

$$\Delta E^f = E^r - E^s - \sum_i E_i. \tag{1}$$

III. RESULTS AND DISCUSSIONS

The $Co(^{tbu2}DAD)_2$ molecule's charge state was first analyzed to identify the molecular characteristics as well as to provide insight

TABLE I. Charge state analysis for the Co atom in the Co(^{tbu2}DAD)$_x$ complex.

Molecule	Magnetic moment (μB)	Charge state
Co(^{tbu2}DAD)$_2$	2.6	2+
Co(^{tbu2}DAD)	2.0	1+
Co	2.5	Neutral

into the possible decomposition mechanisms using spin-polarized density functional methodology.[39] It is shown in Table I that the Co atom donates one electron to each ligand, and this finding agrees well with experimental data.[1] The magnetic moment of the Co atom along with Bader charge analysis was used to identify these charge states. Co(^{tbu2}DAD)$_2$ has a calculated magnetic moment of 2.6 μB, which relates to three unpaired electrons. Co (^{tbu2}DAD) has a calculated magnetic moment of 2.0 μB, which relates to two unpaired electrons, and Co has a calculated magnetic moment of 2.5 μB, which relates to three unpaired electrons.[40] The magnetic moment for Co^{2+} is caused by the loss of the s orbital electrons, thus leaving three unpaired d electrons in the higher energy d_{xy}, d_{xz}, and d_{yz} orbitals. Thus, the lower energy e_g states are fully occupied with four electrons. Co^{1+} shows a lower spin state due to the transfer and pairing of an s orbital electron to the d orbital after the donation of a single s electron to the remaining ^{tbu2}DAD ligand. Lastly, neutral Co should have a magnetic moment of approximately three, which is verified by these data.

The decomposition of Co(^{tbu2}DAD)$_2$ was further studied, and the decomposition in the gas phase is shown in Fig. 1. The first step with 2.475 eV of endothermic reaction energy is the dissociation of the first (^{tbu2}DAD) ligand, forming Co (^{tbu2}DAD) + (^{tbu2}DAD), and the second step with 1.683 eV of endothermic reaction energy is the dissociation of the second (^{tbu2}DAD) ligand, forming Co + (^{tbu2}DAD) + (^{tbu2}DAD). The final step with 0.617 eV of exothermic reaction energy is the *cis–trans* change in DAD geometry. Since the ^{tbu2}DAD ligands are thermodynamically stable even when not a part of the metal complex, it was found that the removal of these ligands is the lowest energy decomposition pathway.[17,41] The thermodynamic energy for ^{tbu2}DAD removal from the Co(^{tbu2}DAD)$_2$ complex is listed in Fig. 1. Here, it is shown that a 2.475 eV reaction energy must be overcome to initiate the thermal decomposition of Co(^{tbu2}DAD)$_2$ in atmosphere, while the total formation enthalpy of Co(^{tbu2}DAD)$_2$ when referenced to ^{tbu2}DAD and single atom Co is 3.541 eV. Therefore, ignoring any ligand–surface interactions which are mentioned later in the text, the Co atom binding energy to a substrate should be larger than 3.541 eV to enable Co(^{tbu2}DAD)$_2$ decomposition leading to Co atom adsorption to the substrate with DAD ligand desorption from the substrate.

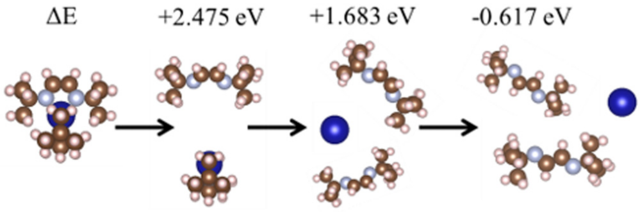

FIG. 1. Decomposition energy and pathway for Co(tbu^{2}DAD)$_2$ in the gas phase. The navy, light blue, brown, and pink spheres represent Co, N, C, and H atoms, respectively. Note there is a *cis–trans* change in DAD geometry in the final step that provides the −0.62 eV change in enthalpy. The overall endothermic reaction energy is 3.541 eV per Co atom.

Furthermore, the formation energy of Co atom deposition on various substrates is listed in Fig. 2. Up to seven Co atoms were used to plot the atom number dependence versus formation energy, as a cluster of seven atoms is required to maximize the number of nearest neighbors of the initial Co atom as illustrated in Fig. 4 for the Cu surface. For the metal substrates, the initial Co adsorption is energetically favorable and there is a gradual increase in formation energy per Co atom with the subsequent adsorption of atoms on the surface. The small difference in the formation energy of Co on the Pt, Cu, and Co substrates is due to the different physical dimensions of the materials. Since Pt has the largest radius, followed by Cu, the Co–Co bonds on the surface become stretched, slightly reducing the formation energy of each Co atom. The surface chemical reactivity also follows the same trend of Co > Cu > Pt, agreeing with increasing Co binding energies on more reactive metal surfaces.

Co adsorption on the SiO_2 surface is described by its own unique characteristics where continuous Co atom adsorption does not result in a steady increase in formation energy. Simulations were conducted on O-terminated $SiO_2(001)$ surfaces, both with (H-SiO_2) and without (SiO_2) H passivation. The increase in formation energy at the beginning results from the formation of CoO_x on the surface through the consumption of weaker bound surface lattice oxygen (on SiO_2) and hydroxyl groups (on H-SiO_2). On H-SiO_2, the interaction with surface hydroxyl groups can result in

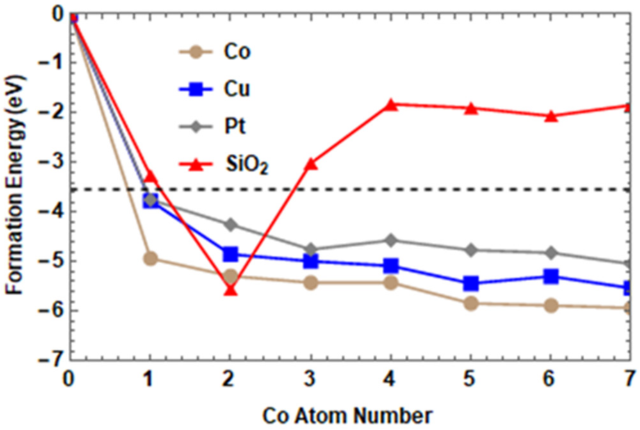

FIG. 2. Formation enthalpy of single Co atom adsorption on Co, Cu, Pt, and SiO_2 substrates are listed for the first seven Co atoms. The reference for the Co atoms is an isolated Co atom. Formation energies greater than the decomposition energy of Co(^{tbu2}DAD)$_2$ (3.541 eV as indicated by the horizontal dashed line) yield Co metal growth on the substrate surface.

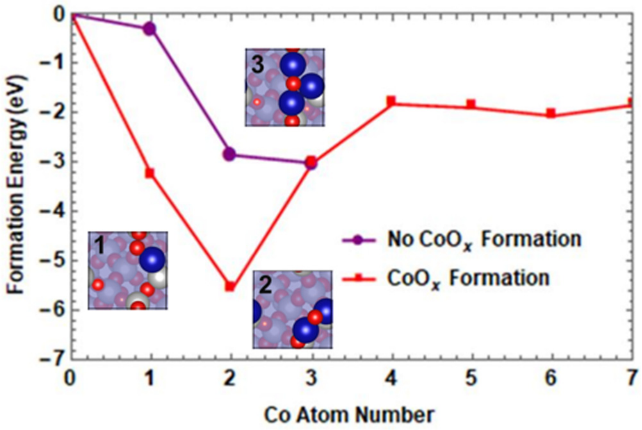

FIG. 3. Formation energies of Co atoms deposited one by one on the SiO_2 substrate are plotted by comparing the energy of Co deposition with and without CoO_x formation. The inner figures depict the formation of CoO_x. The navy, red, and gray spheres represent Co, O, and Si atoms, respectively. Atoms 3–7 are shown to be the same energy because all reactive surface oxygen are already consumed where available, in this particular model.

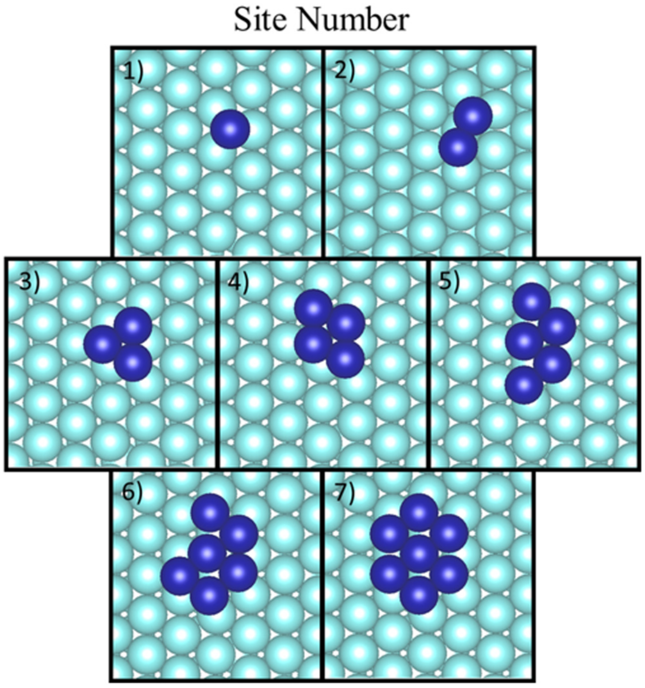

FIG. 4. Atom by atom Co growth on the Cu surface in the most thermodynamically favorable location for each step.

the formation of water as a byproduct, as H atoms migrate from one lattice oxygen to another, allowing the formation of Co–O bonds and H_2O with less favorable energetics compared to SiO_2 (see the supplementary material[43]). However, as additional Co atom deposits and interacts with the surface, the binding energy decreases as the shared surface oxygen and removal of subsequent hydroxyl groups decrease the oxidation state of the surface. This results in the eventual decrease in the formation energy of Co on the surface of SiO_2 as seen in Fig. 2. These later Co atoms no longer chemically bond to the surface oxygen, but rather form a layer of Co that interacts weakly with the surface. For comparison, Co deposited on the SiO_2 surface with and without CoO_x formation is shown in Fig. 3. It is shown that without allowing for CoO_x formation on the surface, Co deposition is thermodynamically unfavorable when compared to the formation enthalpy of Co $(^{tbu2}DAD)_2$ alone (i.e., Co atomic deposition energy <3.541 eV). When comparing the formation energy on SiO_2 and metal surfaces, the energetic characteristics of Co deposition on metal surfaces are similar and have larger formation energy than precursor decomposition energy. Conversely, on SiO_2 and H-SiO_2 surfaces, the formation energy of Co deposition is lower than the precursor's decomposition energy. As a result, the decomposition on metal surfaces is energetically more favorable than on SiO_2 and H-SiO_2, regardless of the formation of CoOx. Note that this does not include the interaction between the surface and the ligands, later shown to be energetically favorable even on SiO_2.

The Co deposition locations on the Cu metal substrate are shown in Fig. 4. Multiple tests were conducted to determine the energetically most favorable configuration. The resulting Co configuration arises from the fact that the adsorbed Co atom forms bonds with both substrate metal atoms and adjacent Co atoms, providing greater bonding characteristics compared to other possible structures. This arrangement and order of adsorption sites proved to be the most favorable on all three metal substrates due to the utilization of the same close-packed (111) surface with different atomic radii. Thus, the Pt and Co substrates showed the same arrangement of Co atoms on the surface at each step, 1–7, with the exception of the Co–Co distance being smaller for the Co substrate and larger for the Pt substrate. Seven deposition steps were chosen because subsequent deposition steps would yield a repeating result.

The electronic density of states (DOS) for the first two Co atoms deposited on Pt, Cu, and SiO_2 are shown in Fig. 5. The DOS for the Co atoms deposited on Pt and Cu substrates shows a small magnetic moment for Co and without any energy gap, both expected characteristics for the Co metal. However, Co deposited on SiO_2 shows the DOS with discrete states and energy gaps. This is indicative of two characteristics for Co adsorption on SiO_2 which vary from the Co deposition on the metal substrates. First, the energy gap is caused by the formation of the insulating CoO_x phase through the consumption of oxygen and surface hydroxyl groups, which are comparatively weakly bound to the surface. This reaction yields CoO_x and some H_2O as byproducts. Second, the discrete nature of the band structure results from the poor hybridization of the Co orbitals and, thus, the formation of molecular-like complexes on the surface and not an extended solid. These insufficient cohesive bonding characteristics best explain the poor affinity of Co for the SiO_2 surface.

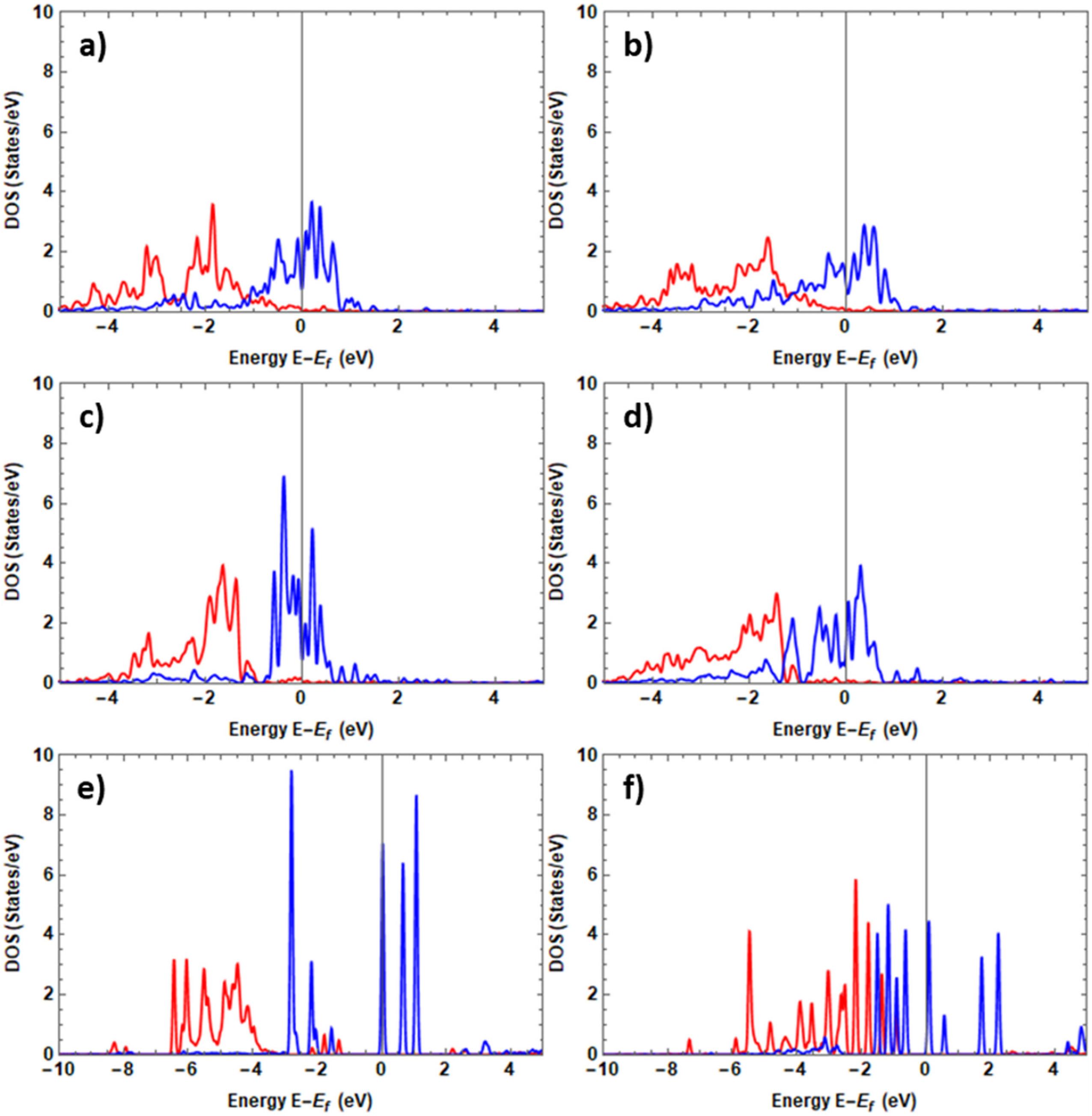

FIG. 5. Density of states (DOS) for the first two Co atoms deposited on Pt, Cu, and SiO_2. These plots are all normalized to 1 Co atom so that the electronic structure is directly comparable. Red and blue represent spin up and down states, respectively. The first and second Co atoms on Pt are shown in (a) and (b), respectively, while the first and second atoms on Cu are shown in (c) and (d), and the first and second atoms on SiO_2 are shown in (e) and (f).

Even though the Co atomic cluster formation energies on metal and SiO_2 surfaces (Fig. 2) are consistent with the experiment data,[19] which shows Co growth on the Cu surface, there is no Co growth on the SiO_2 surface after an initial CoO_x formation. However, there is a required activation step with coreactants in the ALD experiment. Without such an activation step, Co film growth does not happen even on metal surfaces, and the role of the activation step by coreactants is yet to be explained. The activating

TABLE II. Binding energies of the precursor Co(DAD)$_2$ and the coreactant NH$_3$ are listed for Pt, Cu, SiO$_2$, and Co.

	Co(^{tbu2}DAD)$_2$ (eV)	Co(^{tbu2}DAD) (eV)	NH$_3$ (eV)
Pt	−7.01	−4.69	−1.27
Cu	−4.58	−1.84	−0.59
SiO$_2$	−3.07	+0.36	+3.68
Co	−4.85	−2.48	−1.11

coreactant (or reductant) is typically a molecule with a –NH$_2$ group [e.g., (CH$_3$)$_3$CNH$_2$, NH$_3$], and this functional group is known to play the critical activation of Co ALD reactions on metal surfaces. Since the same activating agent does not enable Co ALD growth on the SiO$_2$ surface, which is not thermodynamically favorable, one can speculate that the role of the NH$_x$ group may provide kinetic pathways for Co precursor reactions on metal surfaces. To examine the role of such reductants, we have investigated the effects of NH$_3$ interaction with the metal surface during Co ALD growth, as we discuss now. We first examine the initial precursor and an intermediate reaction product as well as the reactant's interaction with metal and SiO$_2$ surfaces. The formation enthalpies of Co(^{tbu2}DAD)$_2$, Co(^{tbu2}DAD), and NH$_3$ (ammonia) are listed in Table II on the same surfaces as the single atom Co (the final ALD reaction product) formation energies. It is shown that for all the Co complex molecules as well as Co metal atoms (in Fig. 2), the surface interaction is very strong on metal substrates. Furthermore, the exothermic decomposition of NH$_3$ on the metal substrates induces a spontaneous reaction between ammonia and the substrate surface, providing atomic hydrogen on the metal surfaces.[42] However, on the SiO$_2$ surface, the decomposition of Co(^{tbu2}DAD)$_2$ to Co(^{tbu2}DAD) is thermodynamically unfavorable. It is expected that the OH groups on the SiO$_2$ surface may react with the precursor to help facilitate the reaction mechanism. However, in considering the OH interaction with the precursor in DFT calculations, a 1.942 eV endothermic reaction energy was observed to reduce the ^{tbu2}DAD ligands and remove them from the Co complex. The primary reason for this large endothermic reaction energy is the relatively weak reduction of the Co(^{tbu2}DAD)$_2$ precursor in comparison to that of OH. This is one reason for the suppression of ALD reaction and the selectivity of Co(^{tbu2}DAD)$_2$ growth on metal substrates. Additionally, the decomposition of the reductant, NH$_3$, on the surface of SiO$_2$ is highly endothermic indicating that the reductant does not interact with the surface. The reductant is found to play an important role in the growth of Co using Co (^{tbu2}DAD)$_2$, as we discuss now. Due to this catalyzing role of the reductant, the lack of reactant affinity to the surface is another limiting step by itself in the ALD growth of Co on SiO$_2$.

The reaction enthalpies for Co(^{tbu2}DAD)$_2$ growth steps on a Cu substrate (both with and without a reductant, NH$_3$) are shown in Fig. 6. The thermodynamic analysis in Fig. 2 showed the initial and final energies of Co(^{tbu2}DAD)$_2$ decomposition to Co + 2 (^{tbu2}DAD) and Co adsorption to the Cu surface with an overall binding energy of −0.2 eV. The red energy bar in step 10 in Fig. 6 corresponds to this final state of the ALD reaction for a Co (^{tbu2}DAD)$_2$ molecule on the Cu surface. These reaction pathways show the important role of the reductant in Co metal deposition using Co(^{tbu2}DAD)$_2$. For the Cu substrate with NH$_3$ used as a reactant (black bars in Fig. 6), NH$_3$ reacted with the surface prior to the adsorption of Co(^{tbu2}DAD)$_2$ such that the surface was terminated with reactive H and NH$_x$ species. Although most experimental processes expose the surface to Co(^{tbu2}DAD)$_2$ first, this would have no effect on the model, since the Co(^{tbu2}DAD)$_2$–bare surface interaction was also modeled and it was found to have only a physical interaction without a thermodynamically stable decomposition pathway. After one ALD cycle, the substrate would be exposed to reducing molecules, and subsequent cycles happen on the reductant-modified surfaces.

Figure 6 illustrates the reaction steps divided into three distinct sections: (1) long-range molecular–surface interaction, (2) molecular chemical reaction and dissociation on the surface, and (3) desorption of physically bonded ^{tbu2}DAD ligands from the surface. In the first section, step 1 presents the energy for the reference state, where the molecule and surface are positioned infinitely far apart without any interaction. Subsequently, the energies are presented for molecule–surface spacings ranging from 3 to 0 Å in 1 Å increments (steps 2 → 5). These calculations take into account long-range interactions, revealing a significant attraction between the surface and molecule, even in the absence of direct atomic interactions. It is worth noting that the presence of a reductant, NH$_3$, once dissociated on the substrate surface, reduces the surface–molecule interaction compared to a clean surface.

After step 5, the molecule undergoes dissociation on the metal surface in steps 6–9. Step 7 represents the initial loss of ligand from the precursor on the surface, indicating the divergence on two surfaces. For the clean surface (red bars in Fig. 6), the formation enthalpy increases at each subsequent step (5 → 7 → 9). This can be attributed to the decrease in bonding energy between the ligands and Co. While the Co atom forms a strong bond with the Cu surface (∼3.7 eV), the ligands exhibit a weaker physical interaction (∼1.2 eV per ligand) with the substrate surface. This weaker physical interaction is responsible for the energy increase observed in the desorption steps 9 and 10 for both surfaces.

In the case of the NH$_3$ reacted surface, notable changes in enthalpies occur during the chemical reaction steps. Step 6 involves the initial reduction of ^{tbu2}DAD through H donation from the Cu surface. This step exhibits a slight increase in formation enthalpy (0.8 eV) as the molecule transitions from Co bonds to two H bonds, one for each N atom. Step 7 corresponds to the first ligand desorption, where a decrease in energy is observed as Co bonds to the surface and interacts with available NH$_x$ groups on the substrate. Notably, there is a relatively strong physical attraction between the dissociated ligand and the Cu surface, approximately 1.4 eV, resulting in a significant decrease in formation enthalpy for step 7. Steps 8 and 9 involve the dissociation of the remaining Co ligand in a similar manner. However, this time, ligand removal is exothermic due to the weakening of Co-^{tbu2}DAD bonds by the surface–Co interaction.

Finally, step 10 corresponds to the desorption of the ligands into the atmosphere. It is important to clarify that the plotted formation enthalpy does not represent the activation energy. The activation energy is determined by the energy difference between step 4 and step 5, which amounts to 1.1 eV when considering entropy

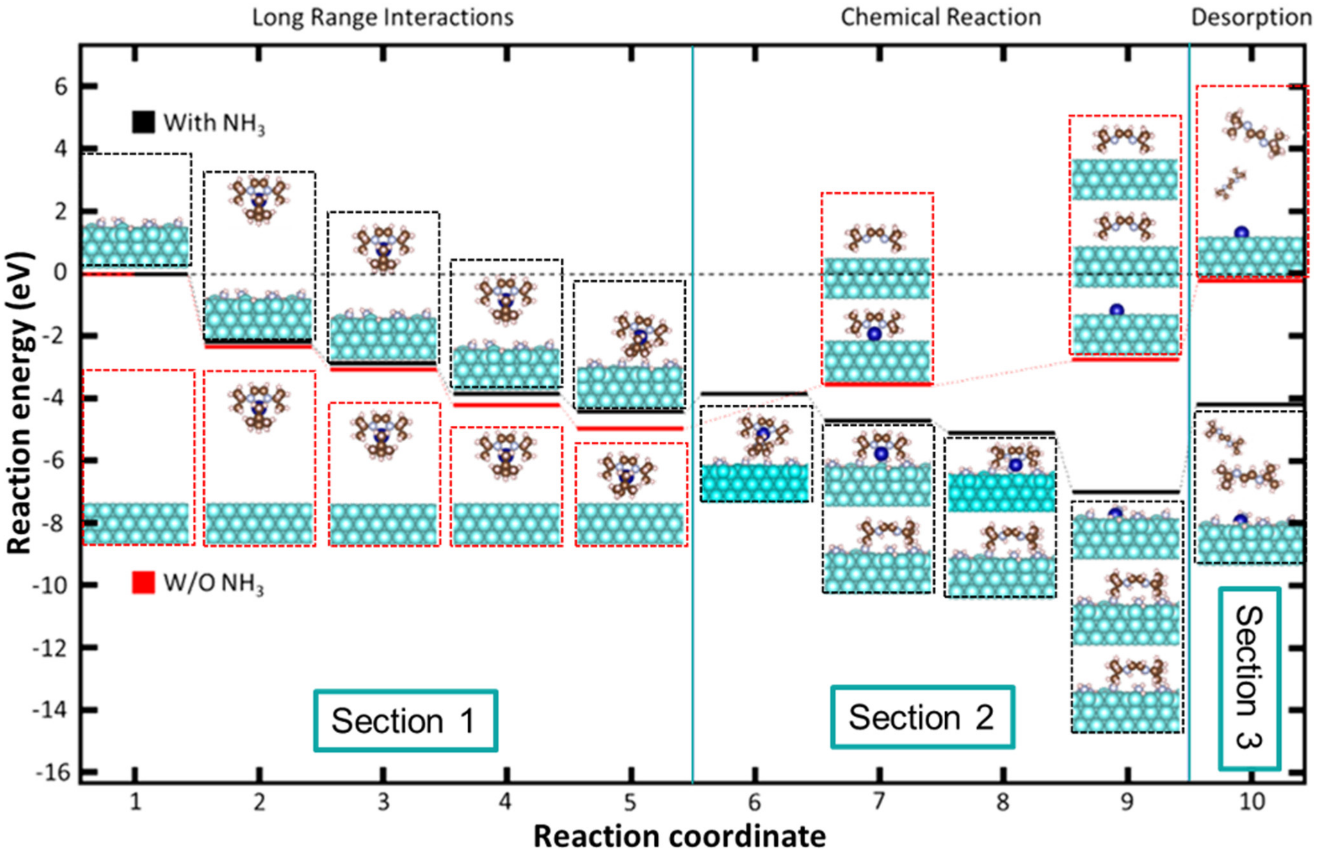

FIG. 6. Step-by-step reaction energetics for Co(^{tbu2}DAD)$_2$ with the Cu surface both with and without a reducing reactant, NH$_3$. The reaction steps are divided into three distinct sections: (1) long-range molecular–surface interaction with closer precursor-surface distance, (2) molecular chemical reaction and dissociation on the surface (steps 7 and 9 are the dissociation of the first and second ligand, the dissociated ligand forms physical interaction with the surface, and steps 6 and 8 are the migration of reactive H from the surface to ligand), and (3) desorption of physically bonded ^{tbu2}DAD ligands from the surface. The structure of each step is shown in the dashed box. The red bars and dashed box represent the energy states and structure for Co reaction with the surface without NH$_{3,}$ while the black bars and dashed box represent it with reactive H and NH$_x$ species dissociated from NH$_3$.

contributions at a deposition temperature of 180 °C. The largest energy jump occurs in the last step, which involves the physical desorption of both ^{tbu2}DAD ligands. This energy jump is twice the reaction energy required for ligand desorption. It is worth noting that this final step does not impact the adsorption of Co, but rather represents the energy difference as the ligands move infinitely far away from the surface.

The role of NH$_3$ as a reductant on the metal surface is highlighted in the following context. Initially, the reductant aids in stabilizing the ^{tbu2}DAD ligands in the atmosphere by facilitating the formation of N–H bonds through the migration of surface reactive H atoms to the Co(^{tbu2}DAD)$_2$ molecule. This bond formation promotes the breaking of Co–N bonds within the molecule. Furthermore, substantial stabilization is achieved through the interaction between the Co atom and NH$_x$ groups on the surface, leading to the formation of relatively strong Co–surface bonds that compensate for the broken Co bonds arising from ligand desorption. These combined processes create an environment that reduces the energy required for Co deposition on the metal surface, resulting in the deposition of Co adatoms from the Co(^{tbu2}DAD)$_2$ molecule with a minor thermodynamic energy step of 0.8 eV in step 6. However, in the absence of a reductant reaction on the Cu surface, the thermodynamic energy required for Co adatom deposition from the Co(^{tbu2}DAD)$_2$ molecule is approximately 2.2 eV (steps 5 → 7 → 9). Consequently, the ALD reaction would halt at step 5, resulting in the physical adsorption of Co(^{tbu2}DAD)$_2$ molecules on the Cu surface. The absence of the reductant cycle would lead to complete coverage of the metal surface with these physically adsorbed molecules, obstructing the subsequent ALD cycles. In contrast, on the reductant-modified surface, the Co adatom on the Cu surface is stabilized by approximately 4 eV at the final step 10, attributed to the interactions between the adatom Co and H atoms. As the ALD cycles progress and more Co adatoms accumulate on the Cu surface, Co clusters form (as depicted in Figs. 2 and 3), and the reactive H atoms bind to the surface of these Co clusters, serving as a reductant in the deposition and growth of the Co film.

While the ligand–surface interaction was studied, dissociation on the surface was not considered in depth. Ligand dissociation is often energetically favorable on a metal substrate surface acting as a catalyst for precursor decomposition reactions. Additionally, it is shown that the metal substrates can dissociate the coreactant, NH_3. Consequently, the dissociation of the precursor on the metal substrates may be more favorable than reflected in this work. The desorption of the surface species may also vary and entail many different chemical species reactions. This makes this interaction complex for large molecules like $Co(^{tbu2}DAD)_2$. However, this reaction would only facilitate Co growth and $Co(^{tbu2}DAD)_2$ decomposition on the metal surfaces. As for SiO_2, it is shown that the interaction is weak, and even simple decomposition steps encompass large endothermic reaction energies to overcome. Overall, the relatively strong bonding characteristic and catalytic effect on the metal surface enable the selective adsorption of Co and the deposition of $Co(^{tbu2}DAD)_2$ precursor, compared with the intrinsically insulating and inert SiO_2 surface. The incorporation of reducing agents such as NH_3 further enhances the selectivity by introducing reactive H and NH_x species on metal surfaces, thereby stabilizing the dissociated ligand and Co adatom, and reducing the reaction energy. This creates a favorable environment for achieving the area-selective atomic layer deposition of Co films.

IV. CONCLUSIONS

The reaction mechanism for the selective deposition of the Co film on Pt, Cu, and Co over SiO_2 was studied by DFT calculation, using the precursor, $Co(^{tbu2}DAD)_2$. Co growth on metal substrates was well supported in DFT thermodynamic studies but showed poor nucleation on SiO_2. This selectivity was, in part, due to the role of a reductant on the metal surface when reacting with the Co precursor and ligands. Without complete thermal decomposition, the $Co(^{tbu2}DAD)_2$ molecule showed a weak dissociation energy on the SiO_2 surface. However, the removal of these ligands being catalyzed by the metal substrate, showed a much more thermodynamically favorable process. This inherent selectivity of the precursor is important to the initial deposition of precursor molecules for the subsequent reactions to form Co films. In addition to the precursor selectivity, it is also seen that NH_3 is both inherently selective to the metal substrate surfaces and readily dissociates, providing reactive H atoms on the surface. Although only one of these, the precursor or the coreactant needs to be selective to allow selective growth, the combination of inherent selectivity characteristics of both the precursor and the coreactant inhibits growth on SiO_2, while facilitating the deposition on Pt, Cu, and Co, and thus, provides an explanation for the experimental observations on Co area selective-atomic layer deposition in literature.

ACKNOWLEDGMENTS

This work was supported by ASCENT, one of the six centers in JUMP, a Semiconductor Research Corporation (SRC) program sponsored by DARPA (Grant No. 2018-JU-2776) and National R&D Program (No. 2022M3H4A1A04096496) through the National Research Foundation of Korea funded by the Ministry of Science and ICT.

AUTHOR DECLARATIONS

Conflict of Interest

The authors have no conflicts to disclose.

Author Contributions

Nickolas Ashburn: Data curation (equal); Formal analysis (equal); Investigation (equal); Writing – original draft (equal); Writing – review & editing (equal). **Xiuyao Lang:** Writing – review & editing (supporting). **Sumeet Pandey:** Conceptualization (supporting); Formal analysis (supporting). **Steven Wolf:** Formal analysis (supporting). **Steve Kramer:** Formal analysis (supporting). **John Smythe:** Formal analysis (supporting). **Gurtej Sandhu:** Formal analysis (supporting). **Charles Winter:** Formal analysis (supporting). **Andrew C. Kummel:** Formal analysis (supporting). **Kyeongjae Cho:** Conceptualization (equal); Funding acquisition (equal); Supervision (equal); Writing – original draft (equal); Writing – review & editing (equal).

DATA AVAILABILITY

The data that support the findings of this study are available from the corresponding authors upon reasonable request.

REFERENCES

[1] T. J. Knisley, M. J. Saly, M. J. Heeg, J. L. Roberts, and C. H. Winter, Organometallics **30**, 5010 (2011).
[2] R. Chen, H. Kim, P. C. McIntyre, and S. F. Bent, Chem. Mater. **17**, 536 (2005).
[3] R. W. Johnson, A. Hultqvist, and S. F. Bent, Mater. Today **17**, 236 (2014).
[4] M. Ritala and M. Leskelä, *Handbook of Thin Films* (Elsevier, 2002) pp. 103–159.
[5] J. R. Schneider, C. de Paula, J. Lewis, J. Woodruff, J. A. Raiford, and S. F. Bent, Small **18**, 2105513 (2022).
[6] T. L. Liu, M. Harake, and S. F. Bent, Adv. Mater. Interfaces **10**, 2202134 (2023).
[7] H. B. R. Lee, Chem. Mater. **31**, 1471 (2019).
[8] A. J. M. Mackus, A. A. Bol, and W. M. M. Kessels, Nanoscale **6**, 10941 (2014).
[9] H. B. Profijt, S. E. Potts, M. C. M. van de Sanden, and W. M. M. Kessels, J. Vac. Sci. Technol. A **29**, 050801 (2011).
[10] L. V. Lutsev, A. I. Stognij, and N. N. Novitskii, Phys. Rev. B **80**, 40 (2009).
[11] C. Vo-Van *et al.*, New J. Phys. **12**, 103040 (2010).
[12] C. C. Yang, P. Flaitz, P. C. Wang, F. Chen, and D. Edelstein, IEEE Electron Device Lett. **31**, 728 (2010).
[13] S. Zhu, R. L. Van Meirhaeghe, C. Detavernier, F. Cardon, G. P. Ru, X. P. Qu, and B. Z. Li, Solid State Electron. **44**, 663 (2000).
[14] M. He, X. Zhang, T. Nogami, X. Lin, J. Kelly, H. Kim, T. Spooner, D. Edelstein, and L. Zhao, J. Electrochem. Soc. **160**, D3040 (2013).
[15] C. C. Yang, F. Baumann, P. C. Wang, S. Y. Lee, P. Ma, J. Aubuchon, and D. Edelstein, IEEE Electron Device Lett. **32**, 560 (2011).
[16] W.-Z. Xu, J.-B. Xu, H.-S. Lu, J.-X. Wang, Z.-J. Hu, and X.-P. Qu, J. Electrochem. Soc. **160**, D3075 (2013).
[17] H. Ago, Y. Ito, N. Mizuta, K. Yoshida, B. Hu, C. M. Orofeo, M. Tsuji, K. I. Ikeda, and S. Mizuno, ACS Nano **4**, 7407 (2010).
[18] R. M. H. New, R. F. W. Pease, and R. L. White, J. Vac. Sci. Technol. B **12**, 3196 (1994).
[19] M. Breeden *et al.*, ACS Appl. Nano Mater. **4**, 8447 (2021).
[20] J. P. Klesko, M. M. Kerrigan, and C. H. Winter, Chem. Mater. **28**, 700 (2016).
[21] M. M. Kerrigan, J. P. Klesko, S. M. Rupich, C. L. Dezelah, R. K. Kanjolia, Y. J. Chabal, and C. H. Winter, J. Chem. Phys. **146**, 052813 (2017).
[22] M. M. Kerrigan, J. P. Klesko, and C. H. Winter, Chem. Mater. **29**, 7458 (2017).

[23] M. M. Kerrigan, J. P. Klesko, K. J. Blakeney, and C. H. Winter, ACS Appl. Mater. Interfaces **10**, 14200 (2018).
[24] M. Lee, R. Hidayat, D. K. Nandi, T. H. Kim, Y. Kim, S. Kim, W. J. Lee, and S. H. Kim, Appl. Surf. Sci. **563**, 150373 (2021).
[25] J. Baek, K. Nam, J. yeon Park, and J. H. Cha, Appl. Surf. Sci. **606**, 154695 (2022).
[26] A. Brady-Boyd, R. O'Connor, S. Armini, V. Selvaraju, M. Pasquali, G. Hughes, and J. Bogan, Appl. Surf. Sci. **586**, 152679 (2022).
[27] K. Khumaini, R. Hidayat, T. R. Mayangsari, T. Chowdhury, H. L. Kim, S. I. Lee, and W. J. Lee, Appl. Surf. Sci. **585**, 152750 (2022).
[28] G. Kresse and J. Furthmüller, Comput. Mater. Sci. **6**, 15 (1996).
[29] D. C. Langreth and M. J. Mehl, Phys. Rev. B **28**, 1809 (1983).
[30] S. Dudarev, G. Botton, S. Y. Savrasov, C. J. Humphreys, and A. P. Sutton, Phys. Rev. B **57**, 1505 (1998).
[31] J. P. Perdew, K. Burke, and M. Ernzerhof, Phys. Rev. Lett. **77**, 3865 (1996).
[32] See https://docs.materialsproject.org/methodology/materials-methodology/calculation-details/gga+u-calculations/hubbard-u-values#references for information about U value determination.
[33] L. Wang, T. Maxisch, and G. Ceder, Phys. Rev. B. **73**, 195107 (2006).
[34] See https://next-gen.materialsproject.org/materials/mp-8352?_skip=330&_sort_fields=symmetry.number&chemsys=Si-O for structure information.
[35] M. Klotzsche *et al.*, Dalton Trans. **50**, 10374 (2021).
[36] R. A. Hoyt, M. M. Montemore, E. C. H. Sykes, and E. Kaxiras, J. Phys. Chem. C **122**, 21952 (2018).
[37] L. Wang, T. Maxisch, and G. Ceder, Chem. Mater. **19**, 543 (2007).
[38] S. Lany and A. Zunger, Phys. Rev. B: Condens. Matter Mater. Phys. **78**, 235104 (2008).
[39] J. Li *et al.*, Nat. Commun. **12**, 1 (2021).
[40] See https://www.vasp.at/vasp-workshop/handsonIV.pdf for information about simulated magnetic momentum.
[41] M. K. Wiedmann, M. J. Heeg, and C. H. Winter, Inorg. Chem. **48**, 5382 (2009).
[42] X. Duan, J. Ji, G. Qian, C. Fan, Y. Zhu, X. Zhou, D. Chen, and W. Yuan, J. Mol. Catal. A Chem. **357**, 81 (2012).
[43] See the supplementary material online for energy comparison.